Pentosan Polysulfate Sodium Causes Diminished Function and Subtle Morphological Changes in Retina and RPE of Mice

Preston E. Girardot,[1,2] Xian Zhang,[1,3] Nan Zhang,[1,4] Kevin J. Donaldson,[1,5] Micah A. Chrenek,[1] Jana T. Sellers,[1] Andrew J. Feola,[1,2,6] Jack Papania,[1] John M. Nickerson,[1] Nieraj Jain,[1] and Jeffrey H. Boatright[1,2]

[1]Department of Ophthalmology, Emory University, Atlanta, GA, United States
[2]Center for Visual and Neurocognitive Rehabilitation, Atlanta VA Medical Center, Decatur, GA, United States
[3]Department of Ophthalmology, Second Xiangya Hospital, Central South University, Changsha, China
[4]Department of Ophthalmology, Zhongnan Hospital of Wuhan University, Wuhan, China
[5]Neuroscience Institute, Georgia State University, Atlanta, GA, United States
[6]Department of Biomedical Engineering, Georgia Institute of Technology/Emory University, Atlanta, GA, United States

Correspondence: Jeffrey H. Boatright, Department of Ophthalmology, Emory University, B5511, Clinic B Building, 1365B Clifton Road NE, Atlanta, GA 30322, USA;
jboatri@emory.edu.

Received: September 28, 2023
Accepted: January 31, 2024
Published: February 21, 2024

Citation: Girardot PE, Zhang X, Zhang N, et al. Pentosan polysulfate sodium causes diminished function and subtle morphological changes in retina and RPE of mice. *Invest Ophthalmol Vis Sci.* 2024;65(2):28. https://doi.org/10.1167/iovs.65.2.28

Purpose. There are numerous reports of a distinctive maculopathy in adults exposed to pentosan polysulfate sodium (PPS), a drug prescribed to treat bladder discomfort associated with interstitial cystitis. We tested whether PPS treatment of mice injures RPE or retina to provide insight into the etiology of the human condition.

Methods. Mice were fed PPS-supplemented chow over 14 months. RPE and retinal function was assessed by electroretinography (ERG) regularly. Following euthanasia, one eye was used for sagittal sectioning and histology, the contralateral for RPE flatmounting. ZO-1 positive RPE cell borders were imaged using confocal microscopy and cell morphology was analyzed using CellProfiler.

Results. After 10 months of PPS treatment, we observed diminution of mean scotopic c-wave amplitudes. By 11 months, we additionally observed diminutions of mean scotopic a- and b-wave amplitudes. Analysis of flatmounts revealed altered RPE cell morphology and morphometrics in PPS-treated mice, including increased mean en face cell area and geometric eccentricity, decreased RPE cell solidity and extent, and cytosolic translocation of alpha-catenin, all markers of RPE cell stress. Sex and regional differences were seen in RPE flatmount measures. Shortened photoreceptor outer segments were also observed.

Conclusions. PPS treatment reduced RPE and later retina function as measured by ERG, consistent with a primary RPE injury. Post-mortem analysis revealed extensive RPE pleomorphism and polymegathism and modest photoreceptor changes. We conclude that PPS treatment of mice causes slowly progressing RPE and photoreceptor damage and thus may provide a useful model for some retinal pathologies.

Keywords: pentosan polysulfate, maculopathy, mouse model

Pentosan polysulfate sodium (PPS) is approved by the U.S. Food and Drug Administration (FDA) for the management of bladder pain or discomfort associated with interstitial cystitis (IC). PPS was first used in the 1950s as a thrombolytic and fibrinolytic agent; it is a heparin-like macromolecule. Currently, it is the only FDA-approved pill treatment for IC.[1] The incidence of IC is estimated to be 45 to 300 per 100,000 women and 8 to 30 per 100,000 men, but these estimated may be overly conservative.[2] The drug has been widely prescribed for this disease since its FDA approval in the 1990s. It is estimated that the number of people exposed to the drug over the decades since its approval is in the hundreds of thousands.[1]

PPS is a carbohydrate derivative, chemically and structurally resembling glycosaminoglycans (GAGs). It is similar in structure to the natural GAG coating of the inner lining of the bladder. In IC, PPS may replace or repair the lining of the bladder wall, decreasing its permeability and protecting it from irritants.[3] However, Jain et al. reported a novel maculopathy suggestive of a primary RPE injury in patients with a history of long-term PPS use.[4] The durations of PPS treatments were often extensive, with patients reporting visual deficits sometimes only after a decade of use. Dosages were typically between 200 and 400 mg/d.[4] Four of the six patients reported significant difficulty reading, and all had subjectively prolonged dark adaptation. Nearly all eyes exhibited a characteristic pattern of aberrations on multimodal fundus imaging. These irregularities were observed in color, near-infrared reflectance, and autofluorescence fundus imaging. Subsets

of these patients showed functional deficits in standard automated perimetry, full-field ERG, and multifocal ERG, typically in eyes with more advanced fundus observations. Retinal morphological disruption was also observed by spectral domain optical coherence tomography transverse retinal imaging.

Our primary purpose was to determine whether PPS exposure had effects on retina or vision in mice. If we observed a phenotype resembling the human findings, it would warrant further studies examining the mechanism of action. Furthermore, this work could potentially serve as a novel RPE damage model that can be adopted by other researchers in the field. Although we cannot realistically hope to recreate the expansive time course over which the affected patients took the drug, short-term regimens in rodents can be informative models of slowly progressing diseases. For example, the clinical prevalence of hydroxychloroquine retinopathy is 7.5% at 5 years on the drug and 20% at more than 20 years, yet a rat animal model that recapitulates hydroxychloroquine retinopathy can be achieved in 7 days.[5]

Here we report that long-term dietary treatment with PPS results in retinal function decline in mice. We observed morphological effects that were more subtle than expected but included reduced outer segment lengths as well as disruptions in en face cell geometry of the RPE. We believe that this mouse model can be further optimized to mirror the human condition more closely.

Methods

Animal Models

All mouse handling procedures and care were approved by the Emory Institutional Animal Care and Use Committee and followed the ARVO Statement for the Use of Animals in Ophthalmic and Vision Research. Adult (postnatal day 90) male and female 129S2/SvPasCrl mice were obtained from Charles River Laboratory (Wilmington, MA, USA) and were housed under a 12:12-hour light–dark cycle (7 AM on and 7 PM off). The mice were divided into one of two treatment groups: PPS treated ($N = 10$, 5 of each sex) and vehicle treated ($N = 10$, 5 of each sex). Mice were euthanized with CO_2 from a bottled source in normal room lighting conditions at postnatal day 520. At sacrifice, one eye was fixed by freeze substitution in a methanol solution for sagittal paraffin sectioning and histology (modified from Sun et al.[6]). The contralateral eye was fixed in Z-Fix (AnaTech, Inc., Kalamazoo, MI, USA) for RPE flatmounting.[7] The 129S2/SvPasCrl mouse strain was used; this current work expands on our initial PPS testing, which involved daily intraperitoneal injections of PPS for long periods. The 129S2/SvPasCrl mice are docile, easily handled, and seemed to be less stressed by daily injections than other commonly used strains. We reported the results of those initial experiments at The Association for Research in Vision and Ophthalmology 2019 and 2021 annual meetings [Girardot P, et al.; *IOVS* 2019;60(9):ARVO Abstract 2352; Girardot P, et al.; *IOVS* 2021;62(8):ARVO Abstract 3131].

Drug Administration

PPS (Letco Medical ID# 696022, Decatur, AL, USA) was added to standard mouse chow in special diet formulations. Drug was shipped to TestDiet (Richmond, IN, USA) for the diets to be manufactured at their facility. Mice had ad libitum access to this food or the standard chow (LabDiet Laboratory Rodent Diet, 5001, St. Louis, MO, USA). The supplemented diets provided ascending doses of PPS as follows: 504 mg/kg/d mouse body weight for 4 months (TestDiet 5WQU, Cat no. 1818746-201, 0.315% PPS), then 1 g/kg/d (TestDiet 5WW1, Cat no. 1818910-201, 0.625% PPS) for the next 3 months, and finally 2 g/kg/d (TestDiet 5WY5, Cat no. 1818983-201, 1.25% PPS) for 7 months. Doses were increased to potentially obtain greater effects because initially we did not observe any functional or morphological changes and the animals tolerated the lower doses well. We measured body weight routinely to assess whether mice on the PPS diet gained weight at the same rate as mice lacking PPS in their diet. Animals of all cohorts gained and maintained weight similarly (Supplementary Fig. S1). One male and two females from the control group and two females from the PPS-treated group died or had to be euthanized before the completion of the experiment. The sampling sizes of the in vivo measures reflect the course of when animals were lost. One animal died before the collection of the in vivo data shown in this article. An additional PPS-treated female presented with squinting over the later period of the experiment. Post mortem observation suggested dislocated lenses with associated inflammation, so data from this animal's eyes were excluded from the postmortem analysis.

ERGs

Mouse retinal function was assessed by ERG at monthly or bimonthly intervals. Briefly, mice were dark-adapted overnight. In preparation for ERGs, mice were anesthetized with intraperitoneal injections of ketamine (10 mg/mL: AmTech Group Inc., Carlisle, PA, USA) and xylazine (100 mg/mL; AKORN Animal Health, Lake Forest, IL, USA). Proparacaine (1%; AKORN) and tropicamide (1%; AKORN) eye drops were administered to anesthetize the ocular surface and dilate pupils. A Celeris ERG system was used (Diagnosys, LLC, Lowell, MA, USA). LED flashes were delivered from stimulators resting on the eyes, which also contained the reference electrodes. Scotopic ERG was performed with six flash stimuli of intensities ranging from 0.001 to 10.000 cd·s/m^2. A- and b-wave magnitudes were recorded over 300 milliseconds after a 4-ms flash for the initial five intensities (0.001–1.000 cd·s/m^2). For the 10 cd·s/m^2 flash step, the recording was extended to 5000 ms. C-waves were recorded as the local maximum in the interval between 1000 ms and 5000 ms after the initial flash. All ERG measurements were analyzed as the responses of both eyes from each mouse averaged together.

Histology

Eyes were flash frozen to −80°C in prechilled fixation solution (97% methanol, VWR, Cat#: BDH20291GLP; 3% acetic acid, Cat#: Fisher BP2401-500) and maintained at −80°C for 4 days to allow substitution of water in the tissue with methanol, washed twice with methanol for 20 minutes, washed twice with xylenes for 20 minutes, infiltrated with paraffin twice for 1 hour, and embedded in paraffin (modified freeze substitution method of Sun et al.[6]). The paraffin-embedded eyes were sectioned through the sagittal plane on a microtome at a thickness of 5 µm. Slides with paraffin sections were processed for hematoxylin and eosin (H&E) staining using an automated processor. H&E stained slides

Investigative Ophthalmology & Visual Science

were imaged on a Nikon Ti2 microscope with a DS-Ri2 camera and 20× objective lens.

RPE flatmounts were prepared similarly to our published approach.[7,8] Briefly, the superior side of the eye was marked with a blue Sharpie marker. Globes were fixed in Z-Fix (Anatech Ltd, Battle Creek, MI, USA) for 10 min, and then washed three times with Hank's Balanced Salt Solution (HBSS; Cat. #14025092, Gibco by Life Technologies, Grand Island, NY, USA). The microdissection technique is as follows: extraocular tissue was removed. The center of the cornea was punctured using 3-mm scissors, and four cuts were made extending from the cornea toward the optic nerve. The iris and the neural retina were removed. Four additional cuts were made in each of the four RPE–scleral flaps to enable the tissue to be flattened. After dissection, the tissues were flatmounted, RPE side up, on conventional microscope slides to which a silicon gasket had been applied (Grace Bio-Labs, Bend, OR, USA). The flatmounts were rinsed with HBSS, followed by incubation with blocking buffer made with 1% BSA (Sigma, St. Louis, MO, USA) in 0.3% Triton X-100 (Sigma) HBSS solution for 1 hour at room temperature.

The flatmounts were incubated with primary antibodies (1:250 anti-ZO-1, Cat. #MABT11, MilliporeSigma; 1:500 anti-CTNNA1 (catenin alpha 1; a.k.a. alpha-catenin), Cat. #EP1793Y, Abcam, Cambridge, MA, USA) overnight at room temperature. On the second day, the flatmounts were washed five times with 0.1% Triton X-100 in HBSS buffer, and then incubated with secondary antibodies (Alexa Fluor 488,1:1,000 donkey anti-rat immunoglobulin G, Cat. #A21208, Thermo Fisher Scientific, Waltham, MA, USA; Alexa Fluor 568, 1:1,000 goat anti-rabbit immunoglobulin G, Cat. #A11036, Thermo Fisher Scientific) overnight at 4°C. On the third day, the flatmounts were washed with Hoechst 33258 (1:250, Cat. #H3569, Thermo Fisher Scientific) in blocking buffer three times, and then washed with HBSS in 0.3% Triton X-100 twice. Next, they were mounted with two drops of Fluoromount-G (Cat. #17984-25, Electron Microscopy Sciences, Signal Hill, CA, USA), coverslipped, and allowed to set overnight. The slides were stored in the dark at 4°C until imaging using a Nikon Ti2 microscope with A1R confocal scanner with a 20× objective lens (Nikon Instruments Inc., Melville, NY, USA) and merged using Nikon NIS Elements software.

Histology Measures and Quantification

Paraffin Sections. We followed the recommendations of Howland and Howland[9] for the nomenclature of axes and planes in the mouse eye. Sagittal sections containing the optic nerve and center of the cornea were selected for staining to ensure that consistent regions were examined between animals. H&E–stained section images were analyzed within ten 100-µm-wide segments spaced approximately 250 µm apart, beginning at a distance of 250 µm superior and inferior of the optic nerve head. Areas of retinal layers were measured in pixels and then divided by the width of the segment to report average layer thicknesses for each segment. Nuclei counts were performed in these sections with the exception of RPE nuclei, which were counted for the entire section. RPE arc length was measured and number of nuclei per micron was reported. Quantified histology measures of the paraffin sections were conducted with ImageJ 1.53.

RPE Flatmounts. Immunostained RPE flatmounts were analyzed using a custom pipeline in CellProfiler 4.1.3 as previously detailed.[7] Eight cut out boxes, four central and four peripheral, were analyzed from each flat mount. Boxes were 372 × 372 µm. The data from the eight boxes were averaged for each flat mount.

Statistical Analyses

Statistical analyses were conducted using Prism 9.5.1 Software (GraphPad Software Inc. La Jolla, CA, USA). Two-way ANOVA with Sidak's multiple comparisons test was used in analyzing ERG data. Unpaired *t* tests, Mann-Whitney *U* tests, and two-way ANOVA with Sidak's and Tukey's multiple comparisons tests were performed when analyzing morphometric and immunofluorescence data. Normality was tested for all datasets in choosing the type of statistical test used. For all analyses, results were considered statistically significant if the *P* value was less than 0.05. All graphs display data as mean ± SEM, except the ERG averaged traces, which are bordered by SDs. The stated *n* is the number of animals used in each group.

Results

PPS Treatment Reduces RPE and Photoreceptor Function in 129SV Mice

Scotopic ERGs were assessed monthly over the course of PPS treatment. No treatment effect was observed up to 9 months of treatment with a PPS-supplemented diet (i.e., after having been fed for 2 months with the highest PPS dose) (Fig. 1). However, at 10 months of treatments, scotopic c-wave mean amplitudes were reduced compared with mice maintained on control diet (Fig. 1B, averaged ERG traces; Fig. 1C, mean c-wave amplitudes at 10 cd·s/m^2 flash intensity) (untreated: 145 ± 7.24 µV vs. treated: 112 ± 5.97 µV; two-way ANOVA with Sidak's multiple comparisons test; $P = 0.0229$). In contrast with diminution of c-wave amplitudes, there were no treatment differences in mean a- or b-wave amplitudes at 10 months of PPS treatment ($P = 0.525$ and $P = 0.491$, respectively Fig. 1A, averaged ERG traces; Fig. 1E, mean a-wave amplitudes and Fig. 1D mean b-wave amplitudes at 10 cd·s/m^2 flash stimulus intensity).

At 11 months of treatment, the mean scotopic a-, b-, and c-wave amplitudes of PPS-treated mice were significantly reduced compared with those of untreated mice (Fig. 1D, 1E, 10 cd·s/m^2 flash stimulus intensity; a-wave untreated: −184 ± 11.0 µV vs. treated: −142 ± 6.63 µV; $P = 0.0069$; b-wave untreated: 568 ± 30.5 µV vs. treated: 441 ± 16.1 µV; $P = 0.0032$; two-way ANOVA with Sidak's multiple comparisons test). Scotopic c-wave amplitudes remained reduced at this timepoint (Fig. 1C, untreated: 131 ± 7.82 µV vs. treated: 97.0 ± 5.36 µV, two-way ANOVA with Sidak's multiple comparisons test; $P = 0.0269$).

Considering ERG responses over the entire study, PPS treatment had a statistically significant main effect on scotopic a-, b-, and c-wave amplitudes, a-waves: $F(1, 81) = 20.35$, $P < 0.0001$; b-waves: $F(1, 81) = 25.19$, $P < 0.0001$; c-waves: F (1, 81) = 3.01, $P < 0.0001$. Also, there was a statistically significant interaction between the effects of PPS treatment and aging on scotopic a-, b-, and c-wave amplitudes, two-way ANOVA, a-waves: $F(4, 81) = 3.01$; $P = 0.0228$; b-waves: $F(4, 81) = 3.09$; $P = 0.0202$; c-waves:

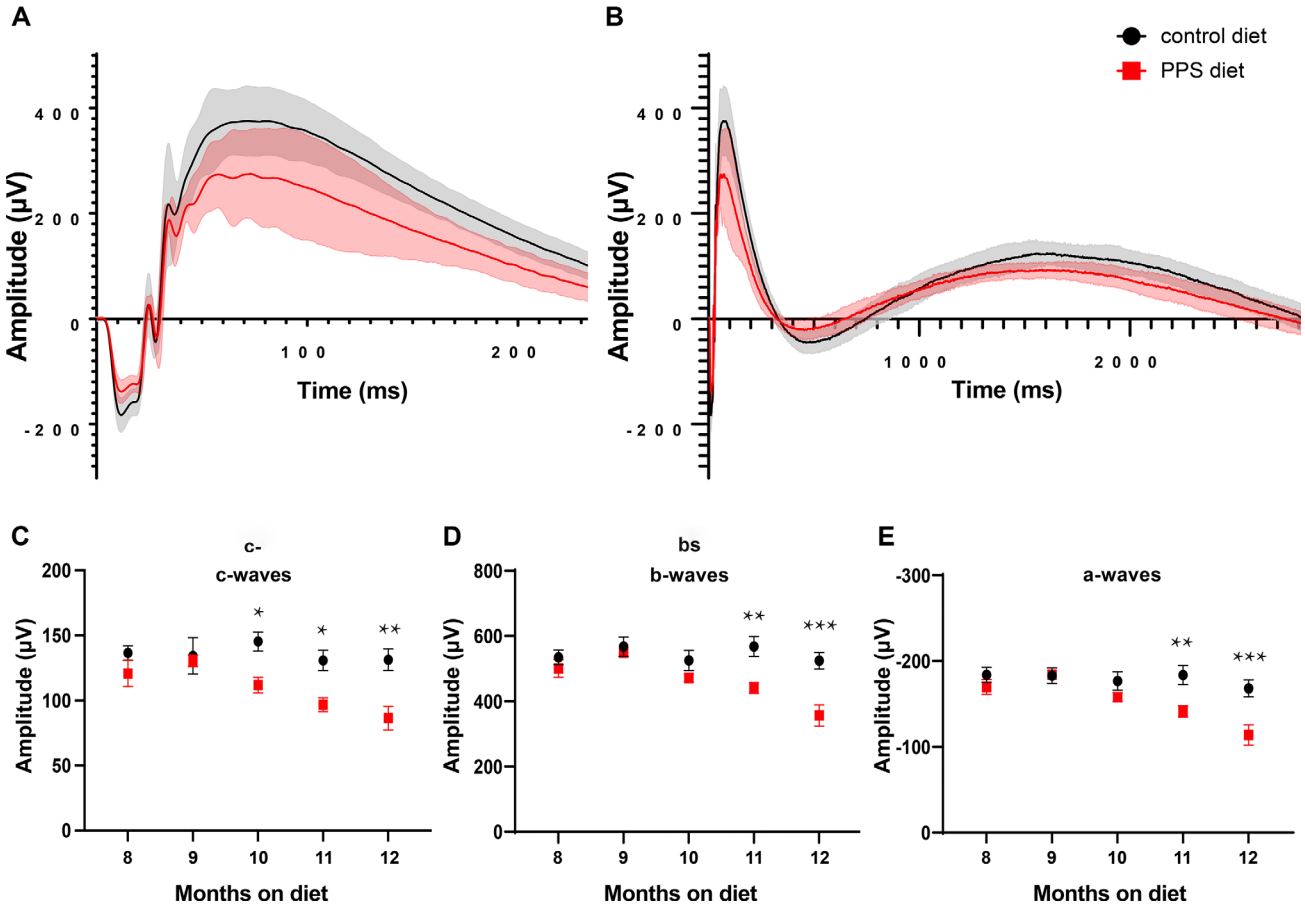

Figure 1. PPS treatment resulted in diminished ERG responses. (**A**, **B**) Averaged ERG traces after 11 months on the three diets (4 months on final, 2 g/kg diet) with SDs shaded (10 cd·s/m^2 flash; *black*, control diet; *red*, PPS diet). (*Bottom*) (**C**) Scotopic c-wave mean amplitudes were reduced after 10 months on the three diets (3 months on the final diet) (**A**, 10 cd·s/m^2 flash, untreated, 145 ± 7.24 μV, treated, 112 ± 5.97 μV, two-way ANOVA with Sidak's multiple comparisons test; $P = 0.0229$). (**D**, **E**) Scotopic a- and b-wave amplitudes were subsequently reduced after 11 months on the three diets (4 months on the final diet) (10 cd·s/m^2 flash, untreated, a-wave, −184 ± 11.0 μV, b-wave, 568 ± 30.5 μV, treated, a-wave, −142 ± 6.63 μV, b-wave, 441 ± 16.1 μV; two-way ANOVA with Sidak's multiple comparisons test; $P = 0.0069$ for a-waves; $P = 0.0032$ for b-waves). n = 8–10, control diet; n = 8–9, PPS diet.

$F(4, 81) = 1.89$, $P < 0.0230$. No sex differences in ERGs were noted with PPS treatment.

PPS-Treated Animals Showed Irregular Morphology of RPE Cells

Postmortem analysis of RPE flat mounts revealed differences in en face cell morphology between the groups. Examples of disrupted cell morphologies are shown in Figures 2B to 2E. RPE cells of PPS-treated mice had mean cell areas of 278.60 ± 6.03 μm^2, a statistically significant increase by more than 245.10 ± 2.05 μm^2 for the age-matched controls (Fig. 2F) ($n_{treated} = 7$; $n_{untreated} = 7$; $P = 0.0002$, unpaired t test). The mean RPE cell eccentricity (the ratio of the distance between the foci of the ellipse best fit to the cell to its major axis length) also was increased in the PPS-treated animals (Fig. 2G) (treated, 0.72740 ± 0.00292, untreated, 0.71170 ± 0.00256; $n_{treated} = 7$; $n_{untreated} = 7$; $P = 0.0016$, unpaired t test). Further, mean RPE cell solidity (the proportion of the pixels in the convex hull of the cell that are also in the cell) and extent (the proportion of the pixels in the bounding box that are also in the cell) were decreased in the treated animals (Figs. 2H, 2I) (solidity: treated, 0.84620 ± 0.00301; untreated, 0.86160 ± 0.00138; extent: treated, 0.60000 ± 0.00395; untreated, 0.62350 ± 0.00156; $n_{treated} = 7$; $n_{untreated} = 7$; solidity: $P = 0.0005$; extent: $P = 0.0001$, unpaired t tests). We previously suggested that translocation of alpha-catenin (CTNNA1) from cell membranes into the cytosol indicates RPE cell stress in mouse models of aging or damage.[10–12] Alpha-catenin typically localizes with ZO-1 at the tight junctions, but in PPS-treated mice, many areas of intracellular alpha-catenin staining were seen across the RPE sheet (Fig. 2J). The mean total intracellular alpha-catenin immunostaining was increased in PPS-treated animals (Fig. 2J) (treated: 45.2 ± 1.52 vs. untreated: 38.5 ± 2.31; $P = 0.0310$, unpaired t test).

RPE differences were more pronounced in the central regions of the flatmounts. Differences in mean en-face RPE cell area, eccentricity, solidity, and extent were limited to the central RPE in the PPS-treated animals (Figs. 3A–D) ($n_{treated} = 7$; $n_{untreated} = 7$; $P < 0.006$, two-way ANOVA with Tukey's multiple comparisons test). Integrated alpha-catenin immunosignal was increased only when the peripheral RPE of the PPS-treated animals was compared with the central

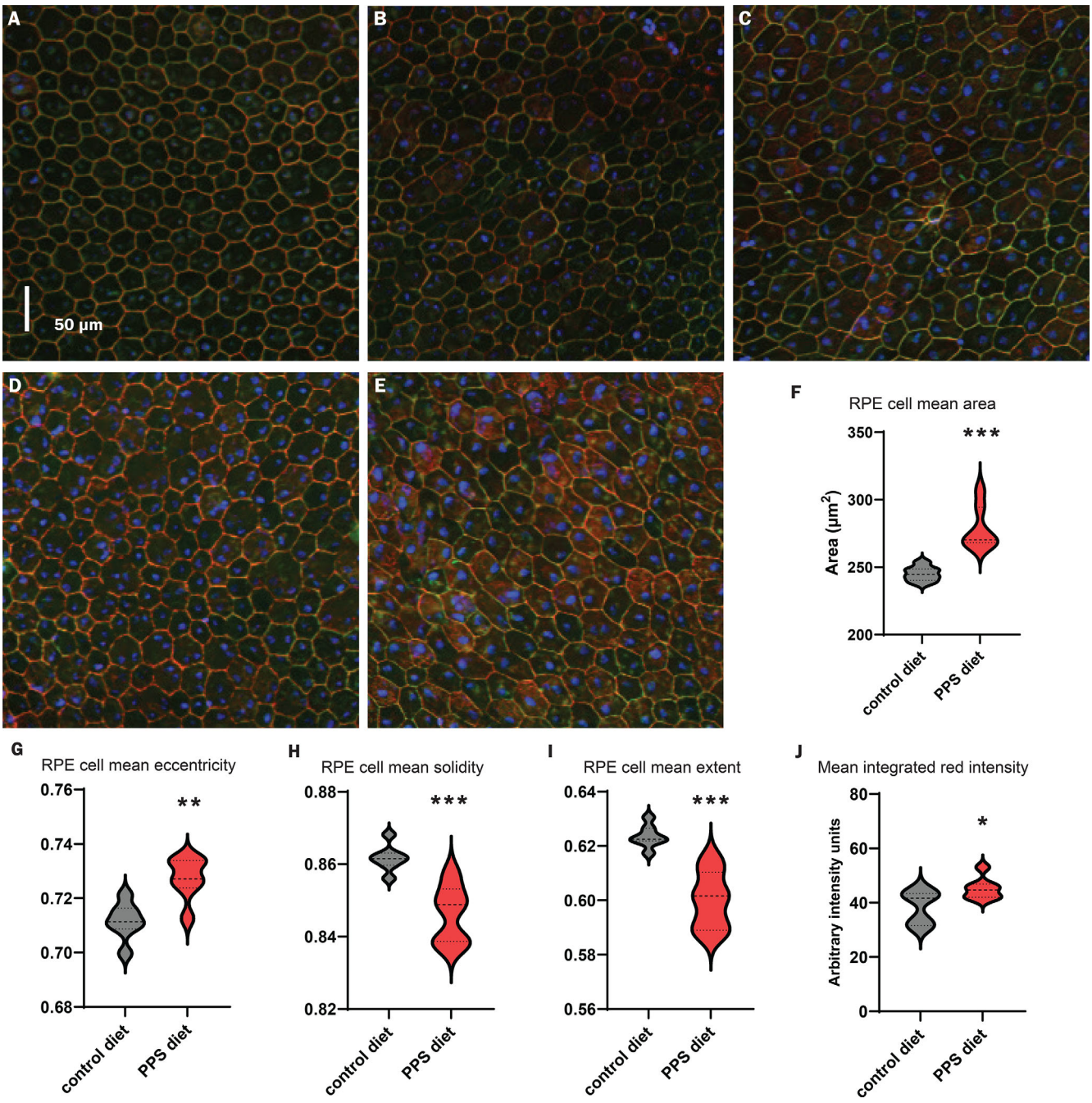

Figure 2. PPS-treated animals had disrupted RPE cell morphology and translocation of alpha-catenin. Images from RPE flat mounts immunostained for ZO-1 (*green*) and alpha-catenin (*red*). (**A**) Example region of interest (ROI) from control diet flat mount. (**B–D**) Representative ROIs from PPS-treated animals. Notice irregular cell sizes and shapes. (**E**) ROI from PPS-treated animal illustrating area of high intracellular alpha-catenin immunostaining. (**F**) PPS-treated mice (*red*) had increased mean en-face cell areas vs. age-matched controls (*gray*) in the RPE sheet ($n_{\text{treated}} = 7$; $n_{\text{untreated}} = 7$; $P = 0.0002$, unpaired t test). (**G**) Mean RPE cell eccentricity (ratio of distance between the foci of the best fit ellipse to the major axis length) was increased in the treated animals ($n_{\text{treated}} = 7$; $n_{\text{untreated}} = 7$; $P = 0.0016$, unpaired t test). (**H**, **I**) Mean cell solidity (the proportion of the pixels in the convex hull of the cell that are also in the cell) and extent (the proportion of the pixels in the bounding box that are also in the cell) were decreased in the treated animals; $n_{\text{treated}} = 7$; $n_{\text{untreated}} = 7$; solidity; $P = 0.0005$; extent; $P = 0.0001$, unpaired t tests). (**J**) Integrated alpha-catenin immunosignal was increased in the PPS-treated animals ($n_{\text{treated}} = 7$; $n_{\text{untreated}} = 7$; $P = 0.0310$, unpaired t test).

RPE of the untreated animals (Fig. 3E) ($P = 0.0371$, two-way ANOVA Tukey's multiple comparisons test). No differences were observed between inferior and superior regions of the RPE.

There were statistically significant sex differences in several RPE measures, with females being more greatly affected, although interpretation should be tempered by modest sampling sizes as noted in the following outcome

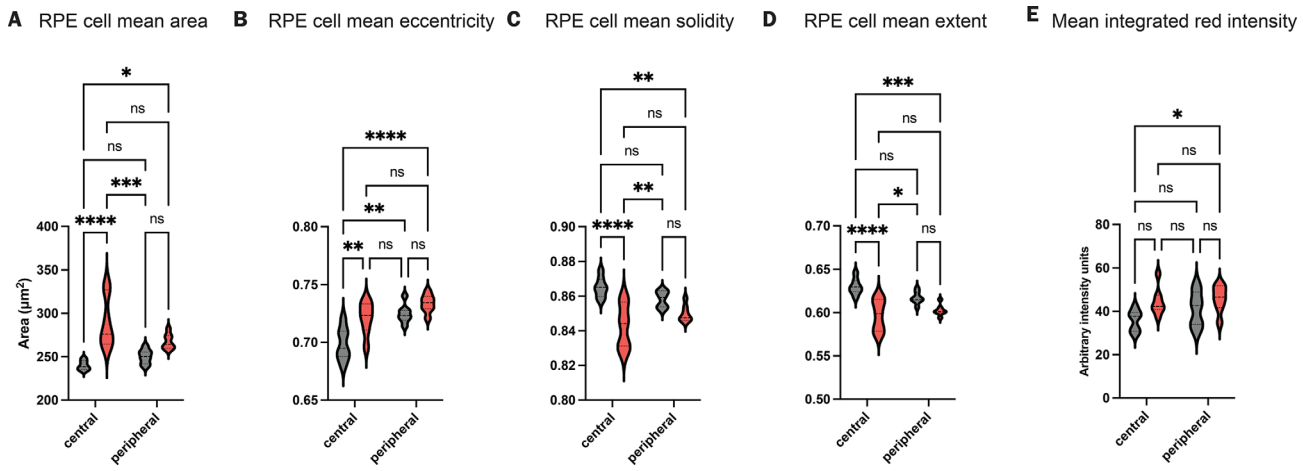

Figure 3. PPS-treated animals (*red*) had more disrupted RPE cell morphology and translocation of alpha-catenin in the central RPE compared with controls (*gray*). (**A**–**D**) Differences in mean en face RPE cell area, eccentricity, solidity, and extent in PPS-treated mice only occurred in the central RPE ($n_{treated} = 7$; $n_{untreated} = 7$; $P < 0.006$, two-way ANOVA with Tukey's multiple comparisons test). (**E**) Integrated alpha-catenin immunosignal was increased only in the peripheral RPE of PPS-treated animals vs. the central RPE of control animals ($P = 0.0371$, two-way ANOVA with Tukey's multiple comparisons test).

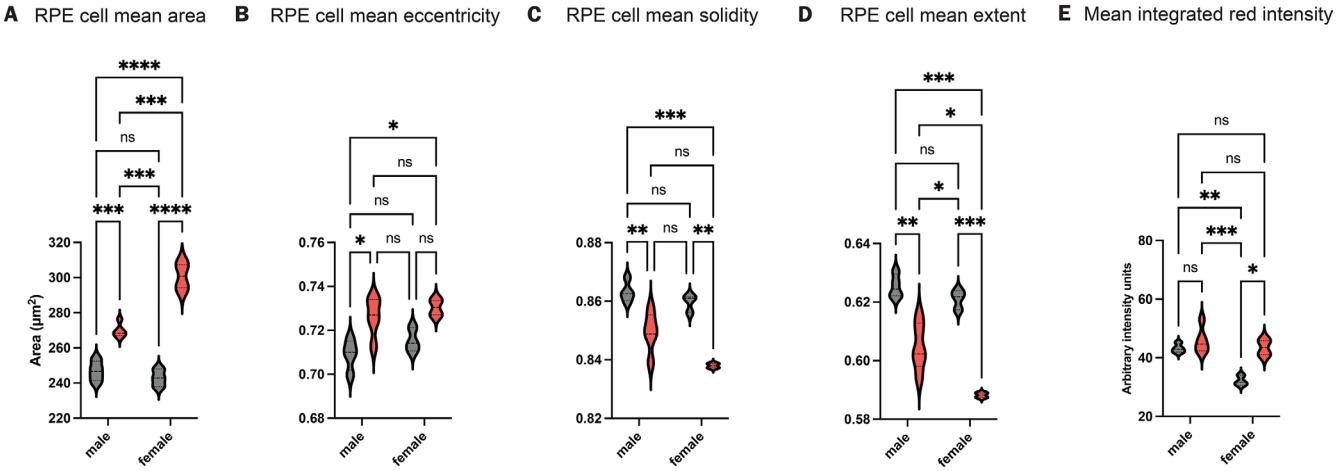

Figure 4. Some RPE changes observed with PPS treatment (*red*) vs. control treatment (*gray*) may be owing to sex differences. There were statistically significant differences in RPE mean cell area and extent in treated females vs. treated males ($n_{male} = 5$; $n_{female} = 2$; $P < 0.03$, two-way ANOVA with Tukey's multiple comparisons test). Treated males had a statistically significant difference in mean eccentricity vs. controls but females did not ($n_{control\ male} = 4$; $n_{treated\ male} = 5$; $n_{control\ female} = 3$; $n_{treated\ female} = 2$; $P = 0.0245$ for males; $P = 0.178$ for females, two-way ANOVA with Tukey's multiple comparisons test). Treated females had a statistically significant difference in mean integrated alpha-catenin immunosignal vs. controls but males did not ($P = 0.611$ for males; $P = 0.0132$ for females). There was an interaction effect between drug treatment and sex on mean cell area and integrated alpha-catenin immunosignal, two-way ANOVA, area: $F(1, 10) = 32.04$; $P = 0.0002$; alpha-catenin immunosignal: $F(1, 10) = 5.767$; $P = 0.0372$.

descriptions. There was an interaction effect between drug treatment and sex on increased mean cell area and integrated alpha-catenin immunosignal (Figs. 4A, 4E), two-way ANOVA, area: $F(1, 10) = 32.04$; $P = 0.0002$; alpha-catenin immunosignal: $F(1, 10) = 5.767$; $P = 0.0372$. Multiple comparisons testing showed significant differences in RPE mean cell area (increased) and extent (decreased) in treated females vs. treated males (Figs. 4A, 4C, 4D; $n_{male} = 5$; $n_{female} = 2$; $P < 0.03$, two-way ANOVA with Tukey's multiple comparisons test). Only males retained the statistically significant increase in mean eccentricity when the sexes were divided ($n_{control\ male} = 4$; $n_{treated\ male} = 5$; $n_{control\ female} = 3$; $n_{treated\ female} = 2$; $P = 0.0245$ for males; $P = 0.178$ for females, two-way ANOVA with Tukey's multiple comparisons test). The opposite is seen in the immunostaining data, where treated females had a statistically significant difference in mean integrated alpha-catenin immunosignal vs. controls but males did not ($P = 0.611$ for males; $P = 0.0132$ for females).

PPS-Treated Mice Had Thinning of the Outer Retinal Layers

Analysis of H&E–stained transverse retinal sections showed that PPS-treated animals had decreased outer segment layer thickness in areas of the central inferior retina (Fig. 5).

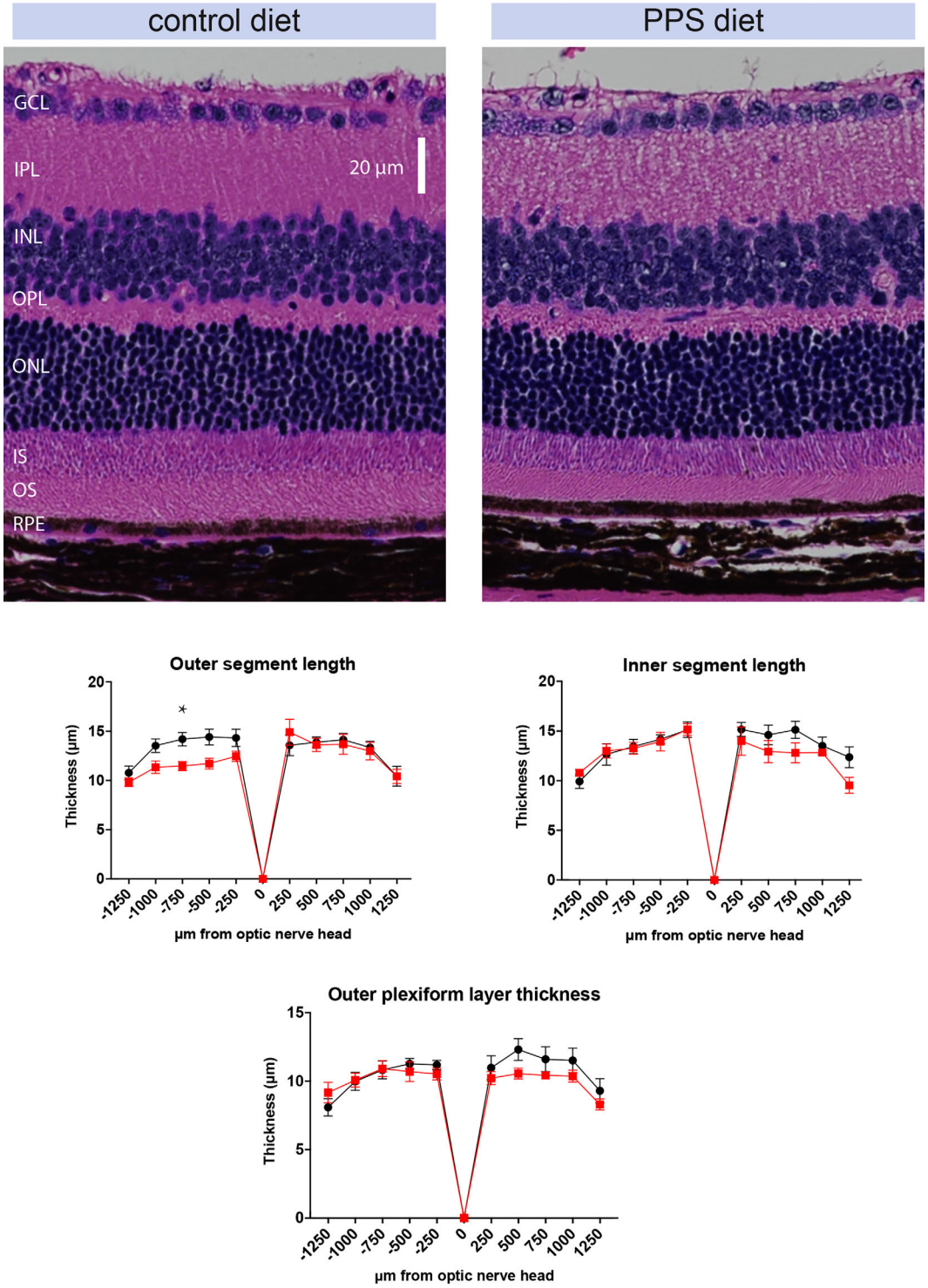

Figure 5. PPS-treated mice had thinner outer segment (OS) layers in the inferior retina. Histology on retinal sagittal sections revealed main drug effects on outer segment length, inner segment length, and outer plexiform layer thickness, two-way ANOVA, outer segment: $F(1, 131) = 8.681$; $P = 0.0038$; inner segment: $F(1, 128) = 4.248$; $P = 0.0413$; outer plexiform layer: $F(1, 127) = 4.159$; $P = 0.0435$. Multiple comparisons testing showed statistically significant decreases in outer segment length in the sector 750 µm inferior to the optic nerve head (untreated [*black*], 14.2 ± 0.677 µm vs. treated [*red*], 11.5 ± 0.458 µm; $P = 0.0471$; two-way ANOVA with Sidak's multiple comparisons test of sectors inferior to the optic nerve head). Negative numbers of the *x*-axis represent the inferior side of the retina; positive numbers represent the superior side.

We observed statistically significant decreases in the sector 750 µm inferior to the optic nerve head (untreated: 14.2 ± 0.677 µm vs. treated: 11.5 ± 0.458 µm; $P = 0.0471$; two-way ANOVA with Sidak's multiple comparisons test of sectors inferior to the optic nerve head). We also observed main drug effects on outer segment length, inner segment

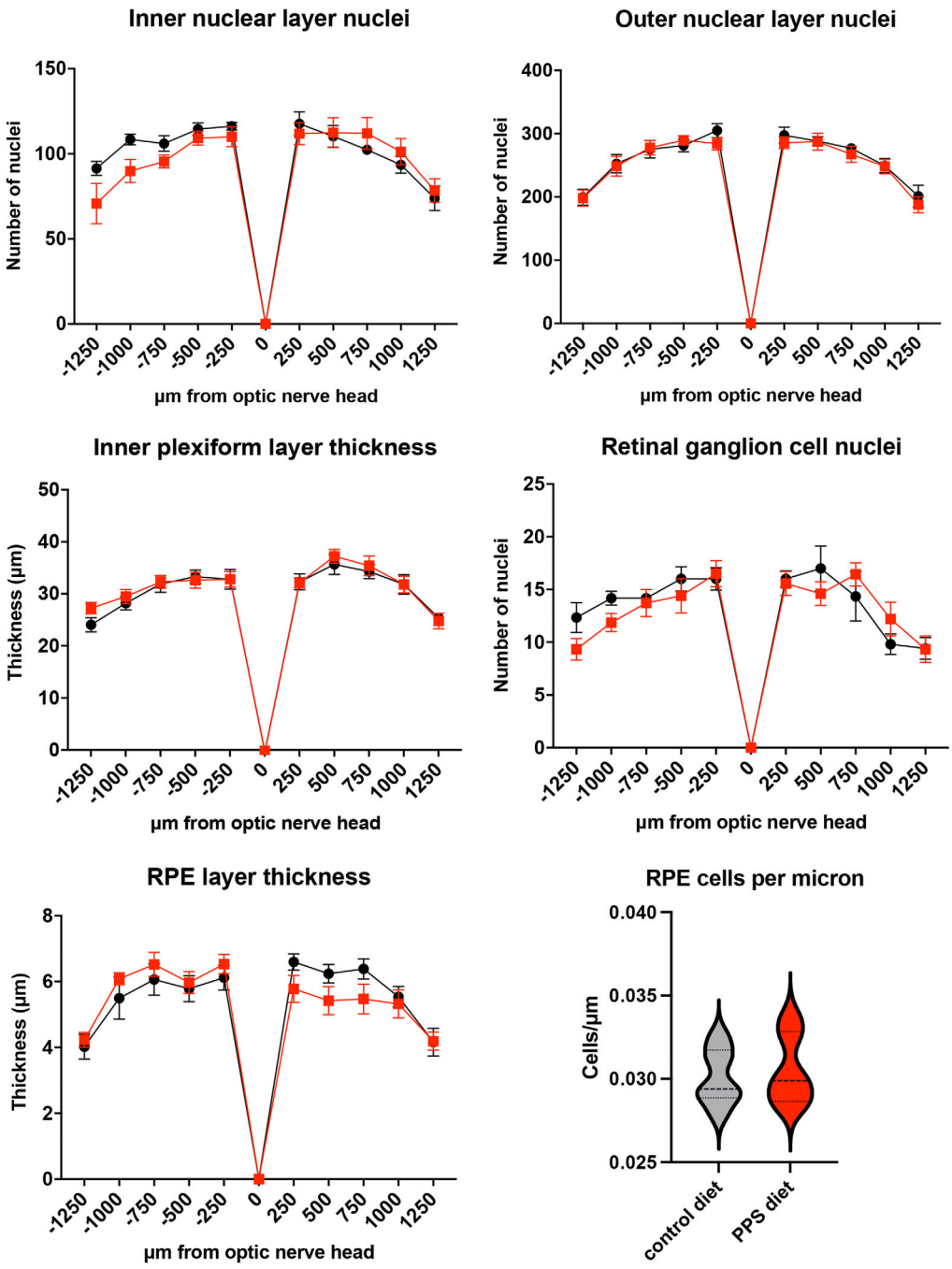

Figure 6. PPS-treated mice had no differences in other sagittal section retinal morphometrics. No statistically significant differences were found in thicknesses of inner plexiform layer and RPE using two-way ANOVA. No differences were seen in nuclei counts of RPE, outer nuclear, inner nuclear, and retinal ganglion cell layers. Total RPE nuclei were counted and then divided by the arc length of the RPE for each paraffin section. Control diet shown as *black* or *gray*; PPS diet shown as *red*.

length, and outer plexiform layer thickness (Fig. 5), two-way ANOVA, outer segment: $F(1, 131) = 8.681$; $P = 0.0038$; inner segment: $F(1, 128) = 4.248$; $P = 0.0413$; outer plexiform layer: $F(1, 127) = 4.159$; $P = 0.0435$. No statistically significant differences were found in measures of other retinal layers using two-way ANOVA (Fig. 6). These factors include thicknesses of the RPE and inner plexiform layers. These also include nuclei counts in RPE, outer nuclear, inner nuclear, and retinal ganglion cell layers. No sex differences were noted.

Discussion

Long-term treatment of mice with PPS resulted in reduced retinal and RPE function as measured by ERG, as well as subtle changes to outer retinal and RPE morphology.

This is similar to clinical findings indicating a retinopathy in patients.[4] Mean scotopic c-wave amplitude was the first parameter observed to be affected, after 10 months on PPS treatment (3 months on the highest dose). The c-wave is a summation of a positive potential from the RPE cells (PI) and a slower negative potential (PIII) from the Müller glia in response to lowered potassium concentration in the interphotoreceptor space after illumination.[13,14] One month later, we observed reductions also in scotopic a- and b-wave amplitudes, indicating impaired photoreceptor and ON-bipolar cell function, respectively. The RPE effects occur before those of the photoreceptors and inner retina. It may be that the RPE is one of the initial ocular sites of PPS-induced functional impairment. These functional losses were not accompanied by significant retinal cell loss, suggesting the possibility that PPS treatment initially disrupts RPE membrane polarity and retinal cell signaling.

We observed RPE cell polymegathisms and geometric eccentricities in our drug-treated animals. This morphology is characteristic of aging and disease, both in mouse and human eyes.[15,16] En face RPE flatmount analyses using CellProfiler revealed statistically significant increases in RPE cell areas. Similar increases in RPE cell area have been reported in aged C57BL/6 mice.[15] We also saw increased intracellular alpha-catenin immunostaining, which we have suggested in reports using a separate RPE damage models of aging and $NaIO_3$ toxicity as being an early, biologically relevant marker for RPE stress.[10–12] This article is the first time we have reported quantified, statistically significant differences in the visualization of this scaffolding protein. These changes in RPE morphology may be signs that the PPS treatment is causing RPE stress and injury. We saw most of these changes only in the central area of the RPE. This result is consistent with our findings in the sodium iodate RPE damage model.[10] We also noted, with the exception of eccentricity, some of these measures showed greater differences among the female mice. This may be reflective of the human condition, because females are more affected by IC and were the majority of patients initially seen with the PPS maculopathy (although it is recognized that the majority of PPS users are female, which may account for sex differences in PPS maculopathy).[2,4]

Another remarkable feature was detected in transverse retinal sections, where we observed that treated animals had reduced outer retinal thickness in the outer and inner segments, as well as the outer plexiform layer. These may indicate disruption of multiple sites on the photoreceptors and their synapses. Reduced outer segment length may be an early biomarker of retinal diseases, including AMD.[17] The RPE in our H&—stained retinal sections did not seem to be remarkable. This finding was unexpected, because patients reported in our initial PPS findings[4] often displayed stark morphological features observed using spectral domain optical coherence tomography, including RPE excrescences and irregularity to outer retinal bands (data not shown). This finding may be attributed to the mouse's lack of a macula or differences in our treatment regimen and/or duration compared with the human patients.

That we only observed RPE and retina effects after escalation of PPS dose may indicate a cumulative dose–response effect. In future studies, we will continue to examine dosing effects; we do not believe that we have seen the full extent of dosing. A longer treatment duration at higher dosages may elicit clear aberrations occurring in at least the RPE that may be observable in vivo. This result would be more in line with the clinical findings.

We did not observe gross systemic effects with PPS treatment. It is thought that PPS decreases the permeability of the bladder to toxins and bacteria by filling in compromised areas of the GAG coating of the urothelium.[18] Bruch's membrane has abundant proteoglycans.[19] Perhaps PPS is aggregating among the GAG chains of these proteoglycans and decreasing Bruch's membrane permeability to nutrients or beneficial factors. It may also be that the PPS or one of its metabolites is passing the blood–retina barrier and acting amid GAGs in the interphotoreceptor matrix, although it has been reported that the drug does not cross the blood–brain barrier owing to its high molecular weight.[20]

PPS may also be sequestering circulating signaling factors. One complement control protein, factor H, is known to bind GAGs.[21] Disruption of the complement system is thought to play a major role in AMD.[22] Although examined, so far we have not noted differential immunostaining for C3, complement factor H, C3aR, and C5aR in our sagittal retinal tissue. Other signaling molecules that could be affecting these changes are the FGFs. These factors regulate angiogenesis and fibrosis, which have major roles in AMD.[23] FGFs interact with GAGs, and, not surprisingly, PPS. PPS has been shown to block the angiogenic effects of FGF2.[24–27] In response to the initial report of PPS-induced maculopathy,[4] Greenlee et al.[28] postulated FGF involvement, citing research on the toxic effects of FGF inhibition on retina in mice and zebrafish.

Although we did not observe gross systemic effects of PPS treatment, it is also possible that the toxic effects from the treatment were a result of decreased hemoglobin. PPS is a heparinoid, and a toxicology study showed that there were statistically significant decreases in erythrocytes and hematocrit in mice gavaged with 500 mg/kg PPS for 3 months.[29] In the toxicology study, these differences were small and did not indicate anemia. In humans, anemia is a rare side effect of PPS, occurring in less than 1% of patients.[30] Although our mice seemed to be healthy throughout the experiment, with no differences in weights among the groups (Supplementary Fig. S1), it may be that the higher PPS dosage resulted in a significant loss of red blood cells. Lowered ERG a- and b-wave amplitudes have been observed in anemic mice.[31] We have observed a slight reduction in hematocrit in more recent experiments (unpublished data, 2023), but the decrease was not as extreme as that observed in the mouse anemia study.[31]

There are, of course, limitations to using mice to model this condition. First and foremost, the human condition is primarily a maculopathy; the mouse does not have a macula. Additionally, a mouse model necessitates a dosing regimen that may differ substantially from human treatments. We cannot duplicate the decades-long drug exposures that some patients experience. Both mice and humans metabolize the drug similarly, excreting approximately 6% in urine,[30] but we provided dosages much higher than those used in human patients to the mice before visual or ocular effects were observed. The final PPS dose used in this study was 2 g/kg/d. This dose corresponds with a human equivalent dose[32] of 162 mg/kg, which is approximately 14× higher than the dose tested in human toxicology studies (i.e., 11.25 mg/kg).[30] A confound may be that our mice did not have any cystitis-like condition. This factor is something we can address in future experiments, because there are mouse models of IC.[33]

Investigative Ophthalmology & Visual Science

The initial intent of these long-term experiments was to balance an equal number of male and female mice in each sample group. Although these experiments were not designed to intentionally analyze for sex-related differences, when we post hoc divided cohorts by sex, we noticed some significant differences, but our experiments were not powered with this work in mind. Our future plans include tests for sex-related differences.

Despite these limitations, we believe that this animal model lends support to recent clinical observations and may suggest a causal relationship between PPS use and this distinctive maculopathy. In the future, we hope to further optimize our model, both to better match the human condition as a new maculopathy model, and to determine underlying molecular mechanisms.

Acknowledgments

Supported by a Challenge Grant from Research to Prevent Blindness, Inc. to the Department of Ophthalmology at Emory University, Foundation Fighting Blindness grant CD-C-0918-0748-EEC (NJ), NIH grants P30EY06360 (JMN and the Atlanta Vision Research Community), R01EY028859 (JHB), R01EY021592 (JMN & JHB), R01EY028450 (JMN & JHB), Veterans Affairs Office of Rehabilitation Research and Development grants RX002806 and RX001924 (JHB), Rehab R&D Service Career Development Award RX002342 (AJF), and the Abraham J and Phyllis Katz Foundation (JHB).

Disclosure: **P.E. Girardot**, None; **X. Zhang**, None; **N. Zhang**, None; **K.J. Donaldson**, None; **M.A. Chrenek**, None; **J.T. Sellers**, None; **A.J. Feola**, None; **J. Papania**, None; **J.M. Nickerson**, None; **N. Jain**, None; **J.H. Boatright**, None

References

1. American Academy of Ophthalmology. More evidence linking common bladder medication to a vision-threatening eye condition: new study shows about a quarter of patients with significant exposure to the drug show signs of retinal damage. *ScienceDaily*. 2019, www.sciencedaily.com/releases/2019/10/191012141218.htm.
2. Kuret T, Peskar D, Erman A, Veranič P. A systematic review of therapeutic approaches used in experimental models of interstitial cystitis/bladder pain syndrome. *Biomedicines*. 2021;9(8):865.
3. Parsons CL. The therapeutic role of sulfated polysaccharides in the urinary bladder. *Urol Clin North Am*. 1994;21(1):93–100.
4. Pearce WA, Chen R, Jain N. Pigmentary maculopathy associated with chronic exposure to pentosan polysulfate sodium. *Ophthalmology*. 2018;125(11):1793–1802.
5. Mahon GJ, Anderson HR, Gardiner TA, McFarlane S, Archer DB, Stitt AW. Chloroquine causes lysosomal dysfunction in neural retina and RPE: implications for retinopathy. *Curr Eye Res*. 2004;28:277–284.
6. Sun N, Shibata B, Hess JF, FitzGerald PG. An alternative means of retaining ocular structure and improving immunoreactivity for light microscopy studies. *Mol Vis*. 2015; 21:428–442.
7. Boatright JH, Dalal N, Chrenek MA, et al. Methodologies for analysis of patterning in the mouse RPE sheet. *Mol Vis*. 2015;21:40–60.
8. Jiang Y, Qi X, Chrenek MA, et al. Functional principal component analysis reveals discriminating categories of retinal pigment epithelial morphology in mice. *Invest Ophthalmol Vis Sci*. 2013;54(12):7274–7283.
9. Howland HC, Howland M. A standard nomenclature for the axes and planes of vertebrate eyes. *Vision Res*. 2008;48:1926–1927.
10. Zhang N, Zhang X, Girardot PE, et al. Electrophysiologic and morphologic strain differences in a low-dose $NaIO_3$-induced retinal pigment epithelium damage model. *Transl Vis Sci Technol*. 2021;10(8):10.
11. Zhang X, Girardot PE, Sellers JT, et al. Wheel running exercise protects against retinal degeneration in the I307N rhodopsin mouse model of inducible autosomal dominant retinitis pigmentosa. *Mol Vis*. 2019;25:462–476.
12. Donaldson KJ, Sellers JT, Boatright JH, Nickerson JM.. Alpha-catenin is a novel marker for identifying abnormal morphology following surgical damage of the RPE. *Invest Ophthalmol Vis Sci*. 2017;58(8):624.
13. Pinto LH, Invergo B, Shimomura K, Takahashi JS, Troy JB. Interpretation of the mouse electroretinogram. *Doc Ophthalmol*. 2007;115(3):127–136.
14. Nilsson SE, Wrigstad A. Electrophysiology in some animal and human hereditary diseases involving the retinal pigment epithelium. *Eye (Lond)*. 1997;11(Pt 5):698–706.
15. Rashid A, Bhatia SK, Mazzitello KI, et al. RPE cell and sheet properties in normal and diseased eyes. *Adv Exp Med Biol*. 2016;854:757–763.
16. Bhatia SK, Rashid A, Chrenek MA, et al. Analysis of RPE morphometry in human eyes. *Mol Vis*. 2016;22:898–916.
17. Nagai N, Minami S, Suzuki M, et al. Macular pigment optical density and photoreceptor outer segment length as predisease biomarkers for age-related macular degeneration. *J Clin Med*. 2020;9(5):1347.
18. Anderson VR, Perry CM. Pentosan polysulfate: a review of its use in the relief of bladder pain or discomfort in interstitial cystitis. *Drugs*. 2006;66(6):821–835.
19. Kelly U, Yu L, Kumar P, et al. Heparan sulfate, including that in Bruch's membrane, inhibits the complement alternative pathway: implications for age-related macular degeneration. *J Immunol*. 2010;185(9):5486–5494.
20. Mead S, Tagliavini F. Human prion diseases. In *Handbook of Clinical Neurology*. New York: Elsevier; 2018.
21. Clark SJ, Bishop PN, Day AJ. Complement factor H and age-related macular degeneration: the role of glycosaminoglycan recognition in disease pathology. *Biochem Soc Trans*. 2010;38(5):1342–1348.
22. Zipfel PF, Lauer N, Skerka C. The role of complement in AMD. *Adv Exp Med Biol*. 2010;703:9–24.
23. Ng EW, Adamis AP. Targeting angiogenesis, the underlying disorder in neovascular age-related macular degeneration. *Can J Ophthalmol*. 2005;40(3):352–368.
24. Marshall JL, Wellstein A, Rae J, et al. Phase I trial of orally administered pentosan polysulfate in patients with advanced cancer. *Clin Cancer Res*. 1997;3(12 Pt 1):2347–2354.
25. Pluda JM, Shay LE, Foli A, et al. Administration of pentosan polysulfate to patients with human immunodeficiency virus-associated Kaposi's sarcoma. *J Natl Cancer Inst*. 1993;85(19):1585–1592.
26. Wellstein A, Zugmaier G, Califano JA, 3rd, Kern F, Paik S, Lippman ME. Tumor growth dependent on Kaposi's sarcoma-derived fibroblast growth factor inhibited by pentosan polysulfate. *J Natl Cancer Inst*. 1991;83(10):716–720.
27. Zugmaier G, Lippman ME, Wellstein A. Inhibition by pentosan polysulfate (PPS) of heparin-binding growth factors released from tumor cells and blockage by PPS of tumor growth in animals. *J Natl Cancer Inst*. 1992;84(22):1716–1724.
28. Greenlee T, Hom G, Conti T, Babiuch AS, Singh R. Re: Pearce et al.: Pigmentary maculopathy associated with

chronic exposure to pentosan polysulfate sodium (Ophthalmology. 2018;125:1793-1802). *Ophthalmology*. 2019;126(7):e51.

29. National Toxicology Program. NTP technical report on the toxicology and carcinogenesis studies of Elmiron, https://ntp.niehs.nih.gov/go/tr512.
30. Ortho-McNeil Pharmaceutical. Elmiron medication guide, https://www.accessdata.fda.gov/drugsatfda_docs/label/2008/020193s007lbl.pdf.
31. Watts MN, Harris NR. Anemia and retinal function in a mouse model of acute colitis. *Pathophysiology*. 2014;21(4):301–308.
32. Nair AB, Jacob S. A simple practice guide for dose conversion between animals and human. *J Basic Clin Pharm*. 2016;7(2):27–31.
33. Birder L, Andersson KE. Animal modelling of interstitial cystitis/bladder pain syndrome. *Int Neurourol J*. 2018;22(Suppl 1):S3–S9.

Investigative Ophthalmology & Visual Science